Biomaterials 31 (2010) 5182–5190

Contents lists available at ScienceDirect

Biomaterials

journal homepage: www.elsevier.com/locate/biomaterials

The functionalization of multi-walled carbon nanotubes by *in situ* deposition of hydroxyapatite

Yu Xiao, Tao Gong, Shaobing Zhou*

School of Materials Science and Engineering, Key Laboratory of Advanced Technologies of Materials, Ministry of Education, Southwest Jiaotong University, Chengdu 610031, Sichuan, PR China

ARTICLE INFO

Article history:
Received 25 February 2010
Accepted 4 March 2010
Available online 13 April 2010

Keywords:
Nanotubes
Biocompatibility
Biomineralization
Hydroxyapatite
In situ

ABSTRACT

A simple and effective approach was introduced to functionalize multi-walled carbon nanotubes (MWNTs) by *in situ* deposition of hydroxyapatite (HA) to improve their hydrophilicity and biocompatibility. Firstly, we prepared two types of pre-functionalized MWNTs: acid-oxidated MWNTs and covalently modified MWNTs by poly (ethylene glycol) (PEG). The influences of the acid-oxidated time, pre-phosphorylation, and PEGylation of MWNTs on *in situ* growth of HA were further investigated in simulated body fluid (SBF) with ionic concentration: 2, 5 and 10 times, respectively, at 37 °C for 24 h. The results exhibited that all these factors have positive effects on the HA crystals growth, especially the PEGylation of MWNTs plays a key role during the deposition. Finally, the methyl thiazolyl tetrazolium (MTT) assay was performed to evaluate their cytotoxicity, which showed that the PEGylated MWNTs wrapped by HA crystals have the best biocompatibility.

1. Introduction

Carbon nanotubes (CNTs) are arousing more and more interests from researchers due to their exceptional combination of mechanical, thermal, chemical, and optical properties [1–3]. Since CNTs are considered as unique materials, they have great potential applications, especially in the field of nanotechnology, nano-electronics, and composite materials [4]. In recent years, the unique properties of CNTs also offer a wide range of opportunities and application potential in biology and medicine. They have already been employed for cancer cell targeting [5,6], intracellular delivery [7], biosensing [8], and imaging [9]. However, there are some drawbacks or problems under debate limited their wide applications in biomedical field. For example, when the CNTs are employed in drug delivery system, a significant limitation has been identified from the pharmacokinetic behavior of carbon nanotubes, owing to their rapid clearance or high hepatic uptake [10,11]. The spread of their use in living systems will require strategies to diminish their cytotoxicity [12]. The previous report related their internalization into living cells indicated that carbon nanotubes can be toxic [13]. The main difficulty to integrate such materials into biological systems derives from their lack of dispersion ability in physiological solutions [4].

To date, raw CNTs are super-hydrophobic and can easily aggregate in aqueous media as well as in organic solvents. Therefore they must be functionalized or modified to improve the hydrophilic and dispersion ability for biological applications. Currently, several strategies based on non-covalent adsorptions or covalent linkages have been developed to functionalize CNTs. For the non-covalent method, agents including anionic, cationic or non-ionic surfactants [14,15], polymers [16–19], biomacromolecules [20–24], and dendrimers [25] have been used. However, the binding affinity between these agents and CNTs' surface is not strong enough by non-covalent interaction, so the hydrophilic and dispersion ability of CNTs in aqueous media are still not satisfied for biomedical application. Therefore, it is necessary to functionalize the CNTs covalently. Chemical modification of CNTs for improving their hydrophilic and dispersion ability has been developed rapidly in recent years. For instance, Zeng et al. have reported the grafting of biodegradable poly (ϵ-caprolactone) onto the surfaces of multi-walled carbon nanotubes (MWNTs) based on *in situ* ring-opening polymerization of ϵ-caprolactone [26]. Sun et al. have reported the covalent functionalization of single-walled carbon nanotubes (SWNTs) with bovine serum albumin or horse spleen ferritin in classical carbodiimide-activated amidation reactions [27,28]. Dai et al. have reported the grafting of short interfering RNA (siRNA) onto the carbon nanotube surface [29]. Polyethylene glycol

* Corresponding author. Tel.: +86 28 87634023; fax: +86 28 87634649.
E-mail addresses: shaobingzhou@swjtu.cn, shaobingzhou@hotmail.com (S. Zhou).

0142-9612/$ – see front matter © 2010 Elsevier Ltd. All rights reserved.
doi:10.1016/j.biomaterials.2010.03.012

modification (PEGylation) to materials surface is a common strategy to impart the materials' functionality, biocompatibility, and hydrophilic. Sun et al. have found that PEGylation of SWNTs is much more effective to achieve prolonged blood circulation and low hepatic uptake [30] than non-covalently PEG-wrapped SWNTs reported by Liu et al. [6]. Until now, covalent attachment of polymers to surface of CNTs has been widely used because the long polymer chains help to dissolve the tubes into a wide range of solvents even at a low degree of functionalization.

Herein, we will report the third approach to functionalize MWNTs by *in situ* deposition of hydroxyapatite (HA) on the materials' surface through the biomineralization method. It is well known that HA, $Ca_{10}(PO_4)_6(OH)_2$ has been currently used in hard tissue engineering such as bone and dentin due to its excellent bioactivity and biocompatibility [31]. Therefore, in recent years, HA has already been considered as an acceptable choice to improve the MWNTs' mechanical properties and decrease the cytotoxicity by a few researchers. For example, Balani et al. have successfully prepared a kind of plasma-sprayed CNTs reinforced HA coatings and systematically investigated the effects of these CNTs with human osteoblasts in vitro [32,33]. Liao et al. have created a self-assembled nano-HA on CNTs and evaluated the morphology and inner structure of crystal HA [34]. There are a few reports concerned about the HA functionalized CNTs, however, it is difficult to find the specific discussions about the properties when the HA deposition on the covalently CNTs, especially on the PEGylation CNTs. On the other hand, the ambient experimental conditions during pre-functionalization and biomineralization process such as acid-oxidated time, pre-phosphorylation and the ionic concentration of simulated body fluid (SBF) are so important that may greatly influence the HA growth. However, these factors are always ignored by many researchers.

In this paper, we firstly prepared two kinds of MWNTs which named acid-oxidated MWNTs (AO-M); poly (ethylene glycol) (PEG) functionalized MWNTs (PEG-M), respectively. Later, the biomineralization method was used to deposit the HA on the surface of PEG-M and AO-M (HA-PEG-M and HA-AO-M), respectively. Moreover, we investigated the effects of acid-oxidated time, pre-phosphorylation and the ionic concentration of SBF during the *in situ* growth of HA process. The morphology and composition of deposited apatite were mainly analyzed by Fourier transform infrared spectroscopy (FT-IR), X-ray diffraction (XRD), field emission scanning electron microscopy (SEM), and transmission electron microscopy (TEM). The water contact angle (CA) was measured to investigate the hydrophilic of these samples. UV–vis absorption spectrum was employed to evaluate the MWNTs' dispersion ability in aqueous system. To accurately determine the actual HA growth rate calculated from the weight change, thermogravimetry differential analysis (TGA) was employed. The cytotoxicity of the functionalized MWNTs was finally evaluated based on the MTT assay evaluation.

2. Materials and methods

2.1. Materials

MWNTs with 10–20 nm outer diameter and 10–20 um length were purchased from Chengdu Institute of Organic Chemistry, Chinese Academy of Sciences. Poly (ethylene glycol) (PEG, $M_n = 2000$ Da) was purchased from Chengdu Kelong Chemical Reagent Company (Sichuan, Chengdu, China). 3-(4, 5-Dimethylthiazol-2-yl)-2,5-diphenyltetrazolium bromide (MTT) was purchased from Sigma. The cells were obtained from the neonatal rat's mandibular osteoblasts. All other chemicals and solvents were of reagent grade or better.

2.2. Processing

Pre-weighed raw MWNTs (Raw-M) were initially added into 70 ml hydrochloric acid (HCl) (36.5 wt%) accompanying with slightly stirring for 2 h, then diluted by water, filtered, washed with deionized water, and dried in vacuum at 40 °C overnight. After that, the pre-treated MWNTs were put into 50 ml nitric acid (HNO_3) (65 wt%) and heated at 140 °C under nitrogen atmosphere for 4 h and then cooled to the room temperature. The above procedures were repeated once. Thereafter, the AO-M samples were prepared.

The synthetic routes for the preparation of PEG-M were shown as Scheme (1) in Fig. 1A. In this reaction we added the N,N-dicyclohexylcarbodiimide (DCC) and 4-dimethylaminopyridine (DMAP) into the AO-M suspension in dichloro-methane (CH_2Cl_2) solvent in order to accelerate the reaction rate and restrict the occurrence of side reaction. The details of this method can be found in the previous literature [35].

The pre-phosphorylation and biomineralization process are displayed in scheme (2) of Fig. 1A. Firstly, phosphorylation was performed for 24 h to all specimens in order to promote the HA deposition. The detailed method for this reaction can be found in the previous report by Michael et al. [36]. Then, these samples were diluted in water, filtered, and washed with deionized water. Finally, each specimen was immersed in 40 ml SBF at 37 °C for 24 h. The SBF with the concentrations of Ca^{2+} and PO_4^{3-} ions 10 times (10×) higher than that of 1.0 SBF (1×) was chosen to fleetly trigger homogeneous nucleation and growth. After 24 h immersion, the resultant MWNTs were filtered, rinsed with distilled water, dried in vacuum at 40 °C overnight, and finally stored in a desiccator.

2.3. Measurements

Nicolet 5700 Fourier transform infrared spectroscopy (FT-IR, Thermo Electron, USA) was performed to identify the attachment of the functional groups on the surface of MWNTs. All specimens were made into powder and mixed with pure KBr at a weight ratio of 0.5–1%. Each sample was recorded from 4000 to 400 cm^{-1} by 64 scans.

The water contact angle (CA) was measured using a sessile drop method at room temperature with the contact angle equipment (DSA 100, KRUSS, Germany). CA values of the right side and the left side of the distilled water droplet were both measured, and an average value was used. The CA was determined at 25 s after the droplet contacted on the surface of the samples. All the CA data were an average of five measurements on different locations of the surface.

The dispersion ability in aqueous system was observed and taken photos after theses samples were added into water and stored for 3 days. The decrease in UV–vis absorption of the solution was used to calculate the average absorption of carbon nanotubes and determine the dispersion ability with UV–visible spectrophotometer (UV-2550, Shimadzu, Japan). The spectra were collected within a range of 200–800 nm, and the maximum absorbance wavelength at 600 nm was employed.

The surface morphology of MWNTs with different treatments was observed using a Quanta200 scanning electron microscope (SEM, FEI, Philips, Netherlands). The specimens were firstly dispersed in water with ultra-sonication for 1 h, and then these specimens were dripped on the pre-cleaned glass fragment. Finally, the specimens were mounted and coated with gold thin layer. The electron accelerating voltage and magnification for SEM were 20 keV and 5000–30,000×, respectively.

The crystalline phases of MWNTs before and after soaked in SBF were identified and compared by XL-30 X-ray diffraction (XRD, Philips X' Pert Pro, Netherlands). The diffractometer with Cu Kα radiation ($\lambda = 1.5406$ Å) from the copper anode source was employed at 40 kV and 40 mA at diffraction angles (2θ) between 10° and 80°, incremented with a step size of 0.03° (2θ) per second.

Transmission electron microscopy (TEM) observation was performed with a HITACHI H-700H at the electron acceleration voltage of 150 kV. TEM samples were prepared by dipping the freshly prepared MWNTs dispersant in aqueous system onto a copper grid with formvar film. A few minutes later, the aqueous solution was blotted away by a strip of filter paper and then dried in air.

Thermo-gravimetric analysis (TGA, Netzsch STA 449C, Bavaria, Germany) was employed to determine the actual yield of HA on the surface of MWNTs. Approximately 10 mg of sample was heated from 20 °C to 900 °C with a heating rate of 10 °C/min in perforated and covered aluminum pans under air purge.

The cytotoxicity of different types of MWNTs was evaluated based on the methyl thiazolyl tetrazolium (MTT) assay. The osteoblasts were grown in RPMI medium 1640 (Gibcos) with 10% fetal bovine serum (FBS). The cells with a density of 1.0×10^4 cells/well were cultured in tissue culture flasks in the above medium and maintained at 37 °C in a humidified incubator with 5% CO_2 and 95% air. After cultured for one day, the culture medium was removed from the cell monolayers cultured in 24-well plates, and each well was reconstituted with 0.2 ml supplemented RPMI-1640 containing 1 mg/ml MTT. After that, the cultures were incubated for 4 h at 37 °C, and the supernatants were removed from the wells. Then, 0.2 ml per well of cell lysing reagent containing 0.04 N HCl in isopropanol was added and mixed with the content of the wells thoroughly. Finally, the plates were read in an automated microplate spectrophotometer at 570 nm as the reference [37]. Every 24 h, the above test was repeatedly performed for totally 72 h.

3. Results and discussion

3.1. FT-IR analysis of pre-functionalized MWNTs

Raw MWNTs (Raw-M) are often modified by chemical treatments, among of which, treatment in HNO_3 is the simplest method

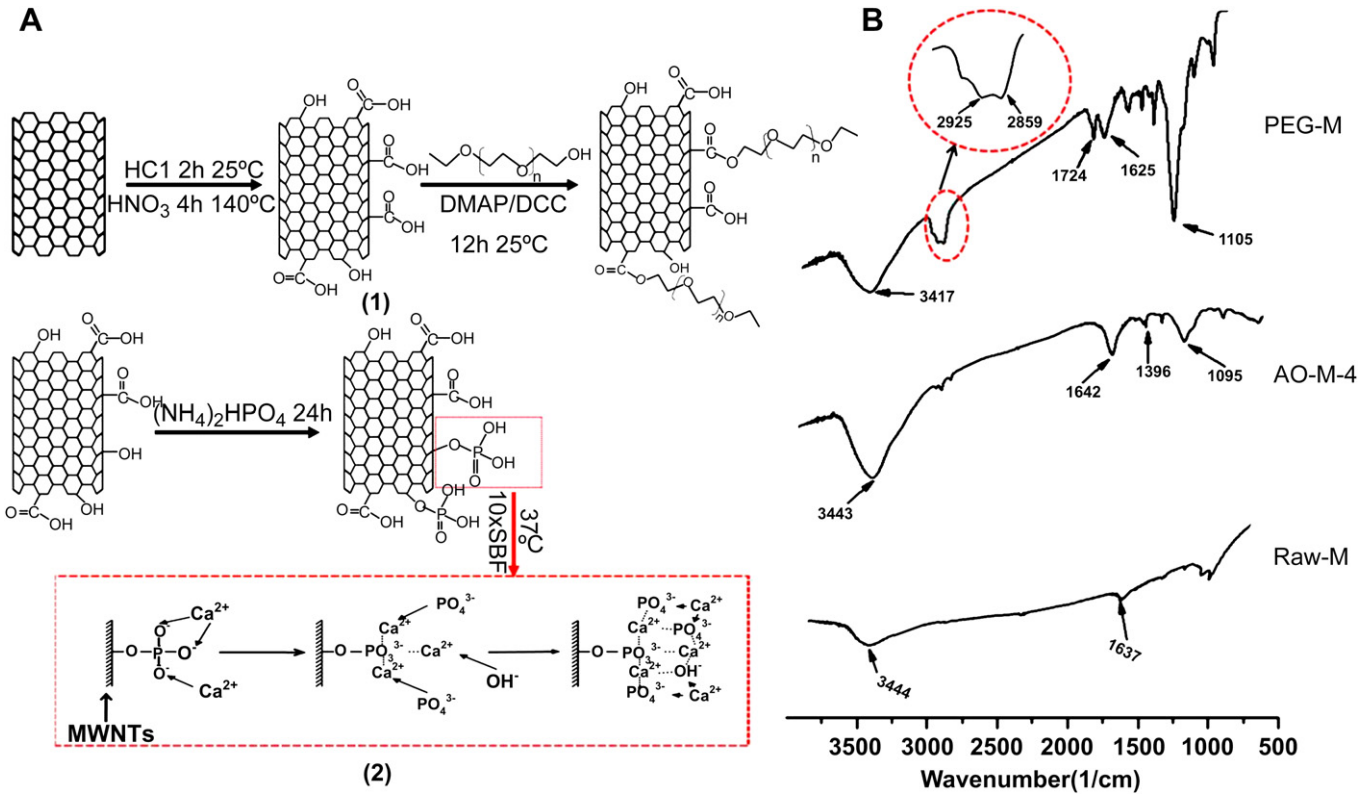

Fig. 1. (A) Scheme of synthetic route for the preparation of PEG-M (1) and the pre-phosphorylation and *in situ* growth mechanism of HA on sidewall of MWNTs (2); (B) FT-IR spectra.

to introduce oxygenated groups such as carboxylic acid groups and hydroxyl groups onto the ends and defect sites of CNTs' surfaces, as reported by Datsyuk et al. [38]. In our report, covalent PEGylation was finally grafted on defects of the sidewall according to Scheme (1) in Fig. 1A. Fig. 1B shows the FT-IR spectra of Raw-M, AO-M and PEG-M, respectively. We can clearly find that the IR absorption spectrum of AO-M mainly consist of the −OH stretch at 3443 cm^{-1}, the carboxyl C═O stretch at 1642 cm^{-1}, and these two characteristic peaks could also be observed in the FT-IR spectrum of the Raw-M. However, the intensity of the two peaks in Raw-M samples' spectrum is much lower than that in AO-M samples' spectrum. Therefore, we could infer the appearance of −OH and C═O in Raw-M is mainly attributed to the non-stoichiometric crystal water in KBr and the original defects on MWNTs and we could further get the conclusion that during the acid-oxidated process, part of the sidewall carbons is indeed oxidized to the carboxyl and hydroxyl groups. From the FT-IR spectrum of the PEG-M sample, we can observe the stretching vibration of the C═O of ester at 1724 cm^{-1} and characteristic absorption peak of C−O−C at 1105 cm^{-1}, which were not present in the absorption spectrum of the other two samples. On the other hand, we could also find the vibration of $-CH_2$ of PEG at about 1080 cm^{-1}. Therefore we can make a conclusion that PEG chains were grafted onto the MWNTs' sidewall successfully.

3.2. Biomineralization

Biomineralization is a quit complicated but powerful approach for the synthesis of advanced materials [39]. Many researchers pay much attention to the mechanism of biomineralization on the different materials' surface, especially based on the CNTs. For example, Akasaka et al. got a conclusion that the CNTs in

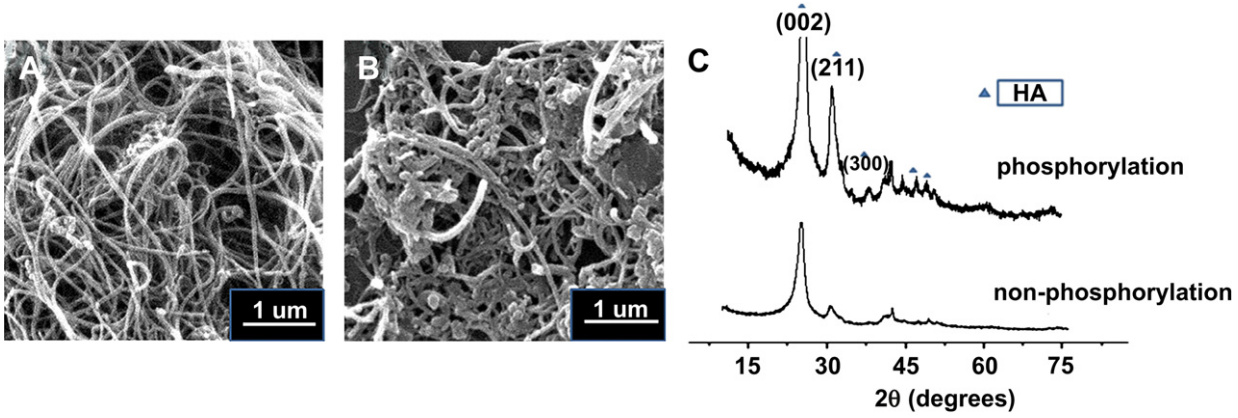

Fig. 2. SEM photos of HA-raw-M without (A) and with phosphorylation (B), XRD patterns of HA-raw-M (C).

biomineralization process may acts as an effective nucleation surface to induce the apatite formation. However, the specific HA nucleation site and the influences of the biomineralization ambient conditions are ignored in their research [40]. In fact, many factors, especially the surface chemistry, can greatly influence the growth rate of the apatite layer [41]. Matsuda et al. found that the type of surface functional groups of the template had great effect on apatite formation in the SBF solution and the group $-H_2PO_4$ would lead to the most satisfying apatite growth rate [42]. Posner et al. further found that the presence of Ca–phospholipid–PO_4 complexes could also cause the hydroxyapatite formation *in vivo* [43].

Therefore, if we expect to get favourable biomineralization results, the $-H_2PO_4$ should be introduced into our system. Thus the pre-phosphorylation was used before the mineralization process. Fig. 2A and B shows the SEM micrographs of HA-Raw-M without and with phosphorylation, respectively. As seen from these images, there was only a little calcium phosphate precipitate formed on the non-phosphorylated MWNTs' sidewall with unfavorable crystal form after 24 h incubation. On the contrary, the growth of apatite crystal favors the surface of the $-H_2PO_4$ functionalized MWNTs. From the macroscopic perspective, the MWNTs with phosphorylation apparently became gray in the solution also suggesting more growth of the clusters of apatite crystallites. The reason can be mainly attributed to the much stronger electrostatic adsorption effect between $-H_2PO_4$ and Ca^{2+} which could effectively trigger the initial step of HA nucleation; Much more deposited position was also produced by the bonded PO_4^{3-} ions that could easily induced the nucleation and growth of HA. This result is also in good agreement with the previous report [43].

In order to estimate the accurate crystal type of calcium phosphate, XRD test was employed. Fig. 2C shows the XRD patterns of the HA functionalized MWNTs with and without the phosphate treatment. As shown in the non-phosphorylated MWNTs profile, there were no distinct peaks appeared for the calcium phosphate except for a weak wide peak at $2\theta = 31.8°$ which was assigned to the non-stoichiometric HA and low-crystalline apatite phase. The XRD profile of the phosphorylated MWNTs displays apparent peaks centered at $2\theta = 31.8°$, 42°, and 47°, which are characteristic patterns of HA. Therefore, the results also strongly proved that phosphorylation process has a positive influence on the growth of HA crystals. In the following studies, all MWNTs were phosphorylated.

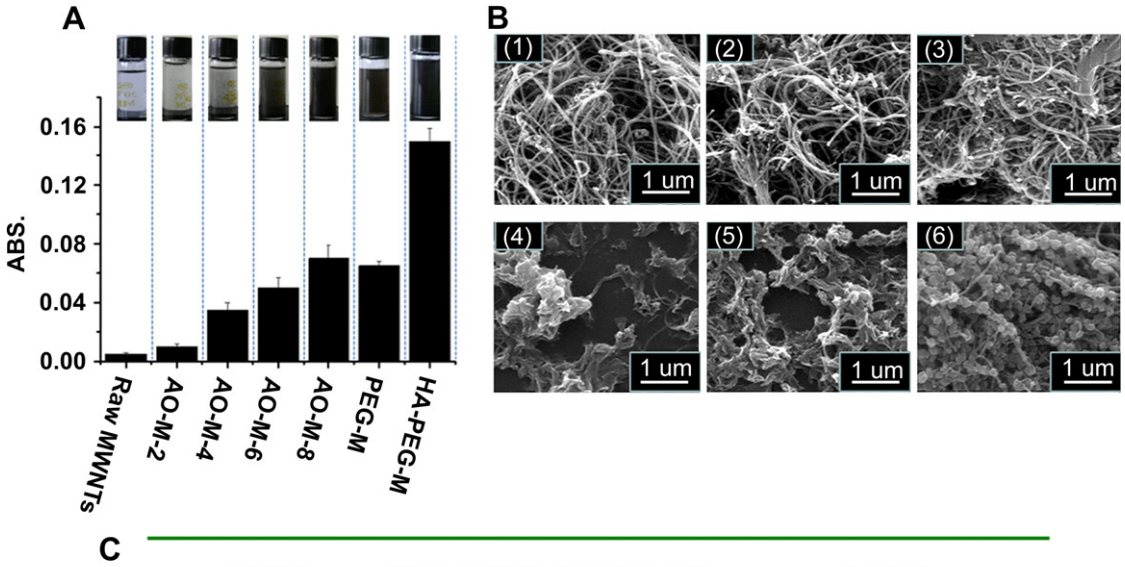

C

samples	water contact angle/deg ±SD	images
Raw-M	109.8±1.5	
AO-M-2	96.4±1.6	
AO-M-4	89.8±1.4	
AO-M-6	84.5±1.5	
AO-M-8	81.9±1.7	
PEG-M	82.2±2.0	
HA-PEG-M	76.3±1.8	

Fig. 3. (A) The dispersion ability in water of all types of MWNTs detected by UV–visible spectrum photometer, (B) SEM photos of HA deposition on Raw-M (1), AO-M-2 (2), AO-M-4 (3); AO-M-6 (4), AO-M-8 (5) and PEG-M (6), and (C) Analysis of water contact angle of all MWNTs.

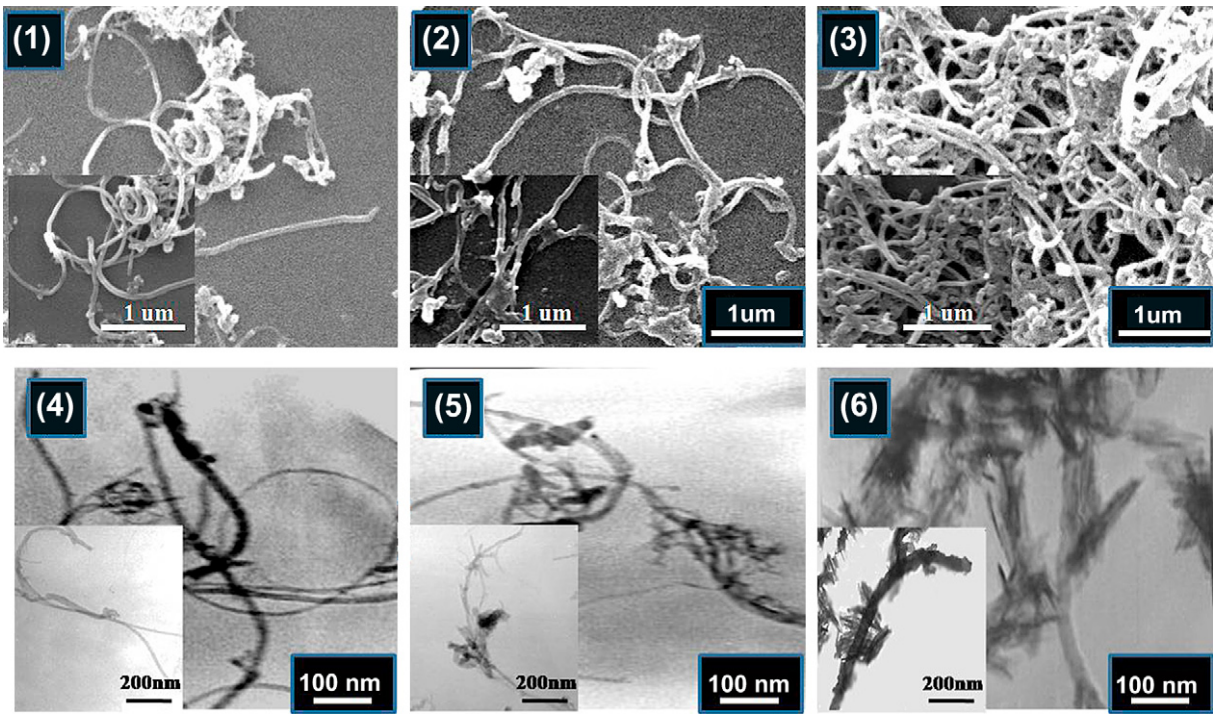

Fig. 4. SEM and TEM photos of HA deposition on AO-M-4 in SBF with three types of ionic concentration: (1), (4) 2×; (2), (5) 5×; and (3), (6)10×, respectively.

The acid-oxidated time is also a very important factor which could lead us to an optimal deposition result. Firstly, the hydrophilic property should be investigated because so many hydrophilic groups have generated during the acid-oxidated process. Fig. 3C summarized the water contact angle data of Raw-M, AO-M with different pre-acid-oxidated time of 2, 4, 6, and 8 h, PEG-M and HA-PEG-M, respectively. From this table, we could find that the Raw-M has quite hydrophobic surface, but its hydrophilic ability has been improved via the acid-oxidated treatment. Simultaneously, from Fig. 3A, we could observe that the Raw-M absolutely precipitate after 3 days standing. Then the absorption data increased with the extension of oxidated time. This result strongly proved the acid-oxidated process could indeed bring the better dispersion ability.

The SEM micrographs provide direct assist to identify the appropriate oxidated time (Fig. 3B). We could see that with the process time passing, the amount of deposited HA increased apparently. TGA analysis also showed that the apatite growth rate largely depended on the oxidated time (Fig. 5D). There were about 7%, 30% and 65% of mineral contents for the MWNTs with the pre-acid-oxidated time of 2, 4 and 8 h, respectively. More oxidated time means more hydroxyl and carboxyl groups and thus more phosphoryl groups can be generated. In other words, more deposited position and higher activation energy of the defects will be appeared in this system to induce the nucleation and growth of HA. However, as some reports we have known that the oxidation process could also bring many defects and damages to the structure of MWNTs, resulting in the fracture of these nanotubes [38]. From these images, we could find the similar phenomenon during our acid-oxidated treatment, especially when the process time beyond 4 h. Therefore, 4 h was selected as the optimal acid-oxidated time in our following experiments.

As mentioned above, the ionic concentrations of SBF is another important factor during the biomineralization process. Fig. 4 shows the SEM and TEM photographs of HA-AO-M after 24 h incubation in SBF with concentration of 2, 5 and 10 times, respectively. The result indicates that higher SBF concentration can lead to the increasing amount of deposited HA. Furthermore, not only the amount of HA increased, but also its crystalline shape improved. From the TEM micrographs we could see many acicular HA crystals grown surrounding the MWNTs when we used the 10 times SBF. This image also proved the work done by Akasaka et al. that the MWNTs may be acting as core for initial crystallization of the apatite [40]. The reason can be summarized as follows: Higher SBF ions concentration brings more Ca^{2+} and PO_4^{3-} in the solution and thus implies higher ion collision probability, in other words, higher ion activation energy. Thereafter the chance of HA nucleation and growth increased significantly.

Through the above comparison and analysis of the MWNTs, we have determined the optimal experimental conditions. However, we can still find that HA growth on MWNTs' surface does not meet the requirement in biomedical field. As it is well known, in nature, organisms could create the proper organic matrix to provide effective help for the nucleation and growth of inorganic crystals. Based on this natural phenomenon, PEGylation to AO-M-4 was conducted in our research.

The formation of calcium phosphate crystals on PEG-AO-M was characterized by FT-IR, XRD, SEM, TEM, and TGA analysis, respectively (Fig. 5A–D). FT-IR spectrum of HA-PEG-M after incubation in 10 times SBF for 24 h is shown in Fig. 5A. The characteristic absorption bands of the apatite phase [44]: the v_4 PO_4 bending band at about 550 cm^{-1} and the –OH stretch band at about 3500 cm^{-1} are present. Ikada et al. reported that the in situ process will facilitate a higher degree of interaction and bonding between the organic and inorganic components of the composite [45]. Here, an important question should be pointed out that after the PEGylation to AO-M-4 and biomineralization, we are not sure that HA was mainly deposited on the MWNTs' surface or the PEG chains? Comparing with the two FT-IR images of PEG-M (Fig. 1B) and HA-PEG-M (Fig. 5B), we could observe two distinct differences before and after the biomineralization process. Firstly, the stretching vibration of ester bond $-COO^-$ at 1724 cm^{-1} in PEG molecule chains disappeared after the HA deposition. Secondly, the intensity

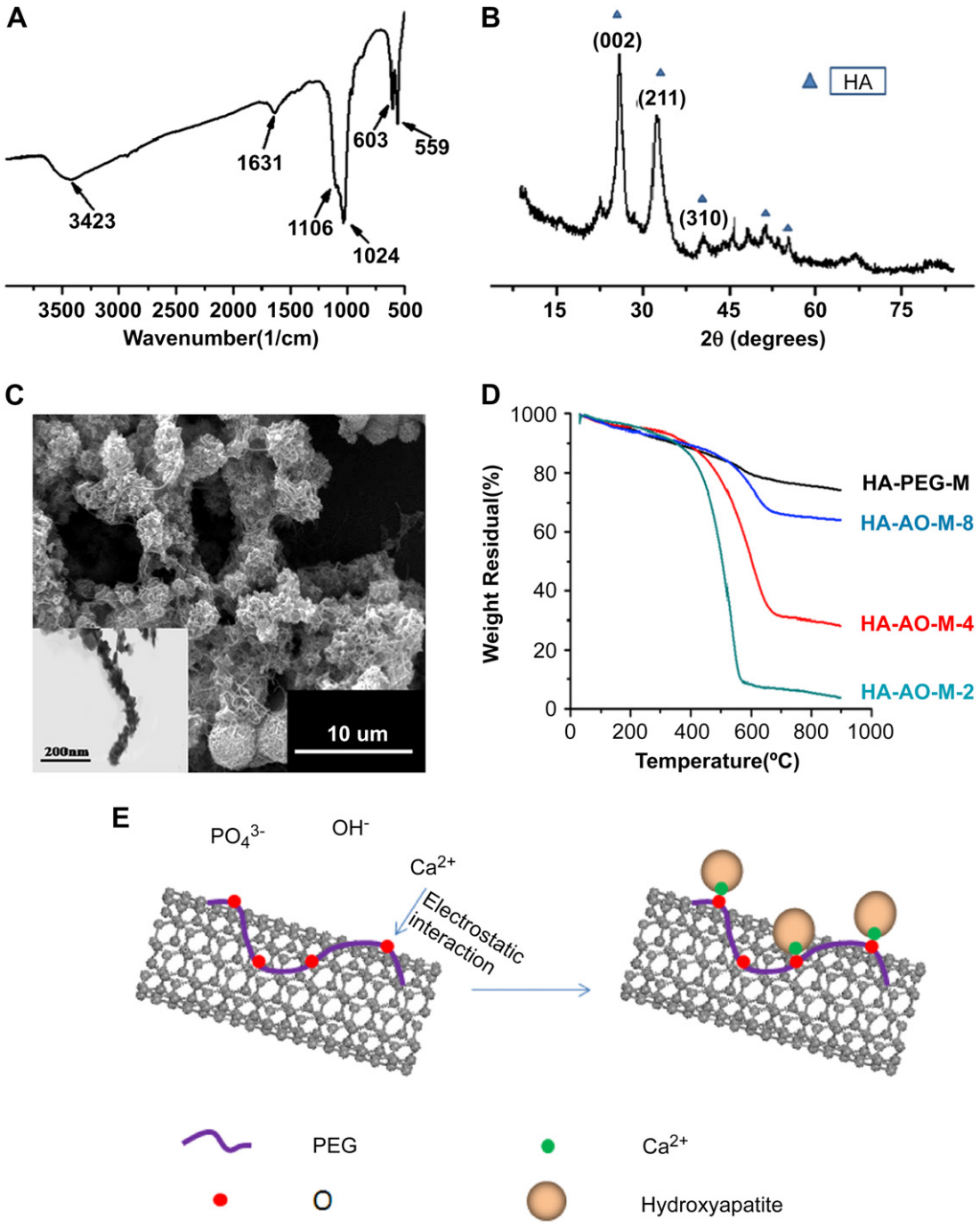

Fig. 5. (A) FT-IR spectrum, (B) XRD pattern, (C) SEM and inserted TEM images of HA-PEG-M, (D) TGA profiles and (E) scheme of biomineralization mechanism of the preparation of HA-PEG-M.

of −C−O−C in PEG chains obviously decreased after the biomineralization. This phenomenon indicates that a kind of interaction existed between HA and the $-COO^{-}$, −C−O−C groups in PEG chains, but not with the −C═O on MWNTs sidewalls. The reason could be explained from the structures and ions properties of MWNTs and PEG chains. There are many interior unsaturated bonds such as C═C in the MWNTs, especially at the defects position. These bonds are usually considered to be electron deficient. Therefore, the direct binding between Ca^{2+} and MWNTs' defects is almost impossible. On the other hand, the oxygen atoms of the −C−O−C− and $-COO^{-}$ in the PEG chains possess many lone pairs of electrons and thus could easily create the ionic interaction with Ca^{2+}. Moreover, as described previously, it may exist a kind of hydrogen bond interaction between the −COO in PEG and −OH in HA which could also enhance the growth of HA [46]. Therefore, we could get the conclusion that the HA is mainly deposited on the PEG chains. The specific mechanism could be referred to the sketch of Fig. 5E. The binding affinity between the HA crystals and the PEGylation MWNTs is strong enough by the ionic and hydrogen bond interaction, which was very helpful to improve the properties and widen the applications of MWNTs. For example, if this kind of HA-PEG-M is used in the drug delivery system, the MWNTs could be considered as the carrier due to their meliorative hydrophilic ability and biocompatibility, and the HA on the surface could also

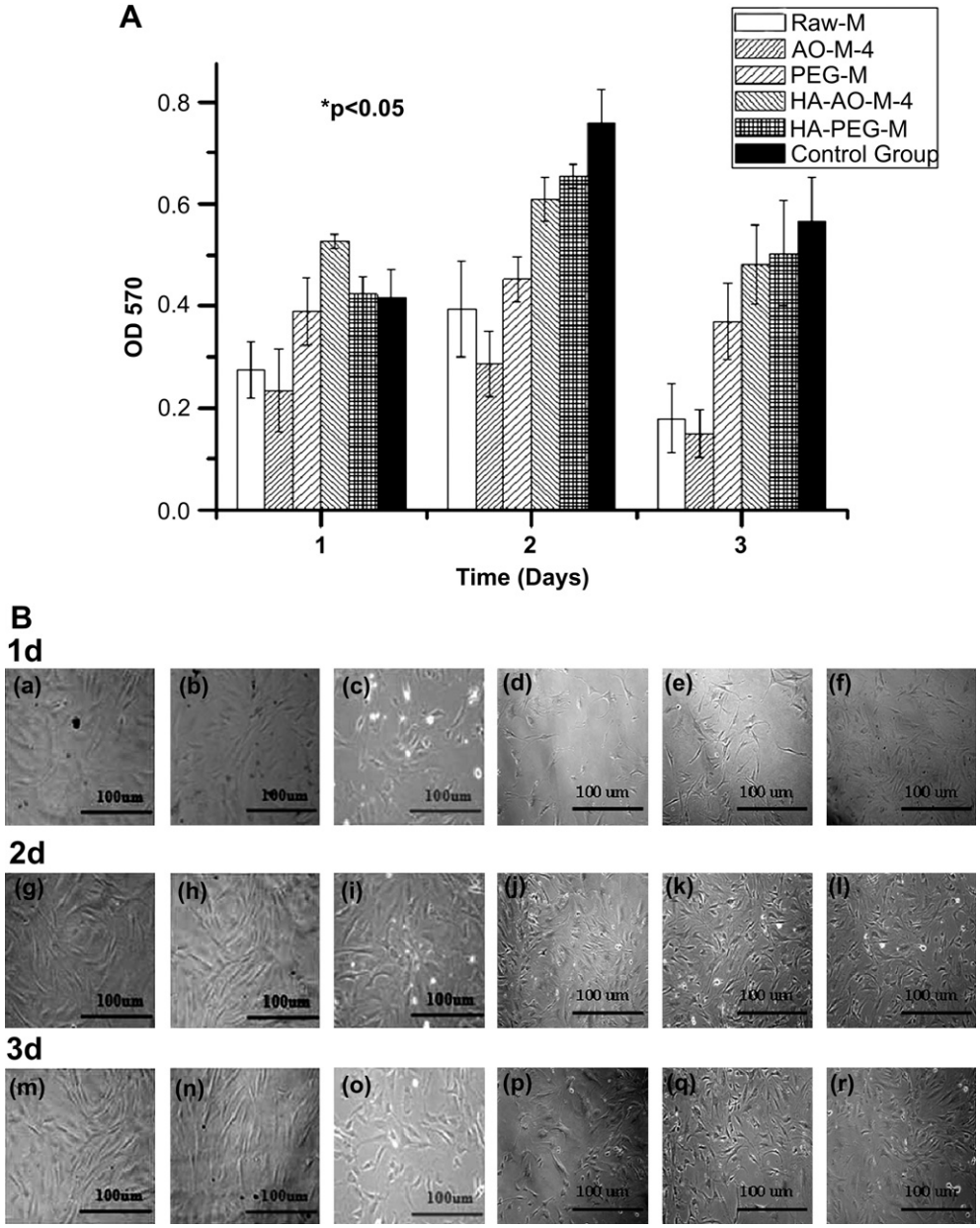

Fig. 6. (A) MTT assay results, (B) optical microscopic observation of osteoblasts growth on Raw-M (a,g,m), AO-M-4 (b,h,n), PEG-M(c,i,o), HA-AO-M-4(d,j,p), HA-PEG-M(e,k,q) and control group(f,l,r) at 1st day, 2nd day and 3rd day, respectively.

be an optimal choice due to its favourable drug-loading capacity and biocompatibility [31,47,48].

Fig. 5B exhibits XRD pattern of crystalline HA on the surface of PEG-M. It is evident that three intense peaks of crystal phases in this sample are around 25.9°, 31.8° and 39.7° 2θ, which are assigned to (002), (211) and (310) of crystalline HA, respectively. Thus, it can be concluded that the crystal phases in this specimen represent the successful mineralization of HA particles. On the other hand, compared with the XRD images in Fig. 2C, we could see that the crystalline peaks of the HA-PEG-M were more integrity than that of the samples without PEGylation, which indicated the crystalline phases of mineralized HA on PEG-M sidewall possessed better crystallizability. It suggests the PEG is a kind of amphiphilic polymers that might control the nucleation and growth of the HA crystals.

As seen from the SEM and TEM images of HA-PEG-M in Fig. 3B and Fig. 5C, the nanotubes were almost wrapped completely by crystals of HA. It is very interesting that this kind of HA possesses spherical shape instead of the traditional needle-like shape. The reason can be located on the following discussion: as shown in Fig. 5E, when the HA-PEG-M samples disperse in the aqueous system, the outer PEG could easily attract the OH^- and further integrate the Ca^{2+} to form PEG–O–Ca^{2+}–O–PEG. This special PEG–O–Ca^{2+}–O–PEG bond is considered as a kind of chelation interaction according to the previous literature [49]. Therefore compared with the traditional HA formation, the new additional PEG will inevitably influence the crystal structure of HA, in other words, will lead to higher HA surface energy. Finally, the shape of HA must spontaneously change to the spherical shape to reduce its high surface energy. Therefore, when the concentration of PEG in this aqueous system achieved a critical level, the HA will exhibit spherical shape. This mechanism has already been proved by a few researchers [50].

TGA analysis displayed that there were about 80% of HA for PEGylated MWNTs (Fig. 5D), which was much higher than other samples. Simultaneously, we can find its dispersion and stability in

aqueous system were also the most excellent (Fig. 3A). Therefore, the graft of PEG chains was indeed able to provide a greater effects for HA crystals to nucleate and grow.

3.3. Cytotoxicity

The cytotoxicity of MWNTs with different treatments (Raw-M, AO-M-4, PEG-M, HA-AO-M-4 and HA-PEG-M) was assessed by a MTT assay, respectively. Our study focuses on the cytotoxicity of HA functionalized MWNTs as the substrates for osteoblasts growth and for bone regeneration. From Fig. 6A, we can see that the Raw-M and AO-M-4 samples performed a certain extent cytotoxicity to reduce the cell viability compared to the control group (control group only contains the RPMI medium 1640 with 10% fetal bovine serum (FBS) and without any additional materials) However, the HA-PEG-M samples exhibited the most favourable biocompatibility in the whole MTT assay process. Thus, the PEGylated and further HA functionalized MWNTs can be suitable for biomedical applications due to the improvement of dispersion ability and biocompatibility. Moreover, it should be noted that the cells counts after 3 days incubation were lower than that of the 2 days incubation. After 2 days incubation, the cells counts achieve a saturated level. After that, a number of cells died due to the limitation of air and nutrition supplies. The cytotoxicity of the MWNTs was also evaluated by optical microscopy analysis (Fig. 6B). The microscopic results closely matched those obtained from the MTT assay. From these images, we can see that the cells morphology of the HA-PEG-M is similar to that of the control group: the amount of the cells became much more than the other four samples and the cells' shape was completely spread out showing a nice grown situation. This result strongly proved that through the process of PEGylation and *in situ* growth of HA, the biocompatibility of MWNTs had been significantly improved. In contrast, for the Raw-M and AO-M-4 samples under similar conditions, the cells became rounded and non-adherent, indicating that there was a significant percentage of cell death.

Therefore, the HA functionalized MWNTs had excellent biocompatibility and dispersion ability in aqueous system, especially after the MWNTs are covalent by PEG. The expected advantages (e.g. excellent biocompatibility and osteoconductivity of HA and the outstanding mechanical property, flexibility and elasticity of MWNTs) could be combined. They may have great potential applications in the field of bone tissue engineering as good scaffold materials for the growth and proliferation of osteoblasts and bone formation. This study may promote and widen the biomedical applications of MWNTs. The HA functionalized carbon nanotubes will play an important role in the research and development of various nanomaterials. Simultaneously, the functionalization strategy could put nanotubes into other biological or biomedical systems.

4. Conclusions

In this study, we mainly investigated the effects of the acid-oxidated time, pre-phosphorylation, PEGylation to MWNTs, and ions concentration of SBF on the crystal growth of HA. The results indicated that all these factors had positive influences on the deposition rate of HA. In particular, covalent PEGylation to MWNTs played a crucial role in the growth of HA crystals. The binding affinity between the HA crystals and the PEG-M surface is strong enough by the ionic and hydrogen bond interactions, which was very helpful to improve the dispersion ability and biocompatibility of nanotubes. Most importantly, the covalently PEGylated carbon nanotubes with HA deposition showed excellent biocompatibility according to the results from the evaluation of MTT assays. Therefore, a simple approach was provided to functionalize carbon nanotubes. It may be of great potential to widen their applications in biomedical field, especially in bone tissue engineering.

Acknowledgements

This work was partially supported by National Natural Science Foundation of China (50773065, 30970723), Programs for New Century Excellent Talents in university, Ministry of Education of China (NCET-07-0719) and Sichuan Prominent Young Talent Program (08ZQ026-040).

Appendix

Figures with essential colour discrimination. Certain figures in this article, particularly Figs. 1–5, are difficult to interpret in black and white. The full colour images can be found in the on-line version, at doi:10.1016/j.biomaterials.2010.03.012.

References

[1] Sun YP, Fu KF, Lin Y, Huang WJ. Functionalized carbon nanotubes: properties and applications. Acc Chem Res 2002;35:1096–104.
[2] Ajayan PM. Nanotubes from carbon. Chem Rev 1999;99:1787–800.
[3] Esawi AM, Farag MM. Carbon nanotube reinforced composites: potential and current challenges. Mater Des 2007;28:2394–401.
[4] Kharisov BI, Kharissova OV, Gutierrez HL, Méndez UO. Recent advances on the soluble carbon nanotubes. Ind Eng Chem Res 2009;48:572–90.
[5] Kam NW, Connell MO, Wisdom JA, Dai HJ. Carbon nanotubes as multi- functional biological transporters and near-infrared agents for selective cancer cell destruction. Proc Natl Acad Sci U S A 2005;102:11600–5.
[6] Liu Z, Cai WB, He LN, Nakayama N, Chen K, Sun XM, et al. *In vivo* biodistribution and highly efficient tumour targeting of carbon nanotubes in mice. Nat Nanotechnol 2007;2:47–52.
[7] Kostarelos K, Lacerda L, Pastorin G, Wu W, Wieckowski S, Godefroy JS, et al. Cellular uptake of functionalized carbon nanotubes is independent of functional group and cell type. Nat Nanotechnol 2007;2:108–13.
[8] Star A, Tu E, Niemann J, Gabriel JC, Joiner CS, Valcke C. Label-free detection of DNA hybridization using carbon nanotube network field-effect transistors. Proc Natl Acad Sci U S A 2006;103:921–6.
[9] Wong SS, Joselevich E, Woolley AT, Cheung CL, Lieber CM. Covalently functionalized nanotubes as nanometresized probes in chemistry and biology. Nature 1998;394:52–5.
[10] Yang S, Wei G, Lin Y, Deng XY, Wang H, Sun HF, et al. Biodistribution of pristine single-walled carbon nanotubes *in vivo*. J Phys Chem C 2007;111(48):17761–4.
[11] Cherukuri P, Gannon CJ, Leeuw TK, Schmidt HK, Smalley RE, Curley SA, et al. Mammalian pharmacokinetics of carbon nanotubes using intrinsic near-infrared fluorescence. Proc Natl Acad Sci U S A 2006;103:18882–6.
[12] Magrez A, Kasas S, Salicio V, Pasquier N, Seo JW, Celio M, et al. Cellular toxicity of carbon-based nanomaterials. Nano Lett 2006;6:1121–5.
[13] Porter A, Gass M, Muller K, Skepper J, Midgley P, Welland M. Direct imaging of single-walled carbon nanotubes in cells. Nat Nanotechnol 2007;2:713–7.
[14] Cherukuri P, Bachilo SM, Litovsky SH, Weisman RB. Near-infrared fluorescence microscopy of single-walled carbon nanotubes in phagocytic cells. J Am Chem Soc 2004;126:15638–9.
[15] O'Connell MJ, Bachilo SM, Huffman CB, Moore VC, Strano MS, Haroz EH, et al. Band gap fluorescence from individual single-walled carbon nanotubes. Science 2002;297:593–6.
[16] Kong J, Franklin N, Zhou C, Chapline M, Peng S, Cho K, et al. Nanotube molecular wires as chemical sensors. Science 2000;28:622–5.
[17] Collins PG, Bradley K, Ishigami M, Zettl A. Extreme oxygen sensitivity of electronic properties of carbon nanotubes. Science 2000;287:1801–4.
[18] Chen J, Liu HY, Weimer WA, Halls MD, Waldeck DH, Walker GC. Noncovalent engineering of carbon nanotube surfaces by rigid, functional conjugated polymers. J Am Chem Soc 2002;124:9034–5.
[19] Shim M, Javey AS, Kam NW, Dai H. Polymer functionalization for air-stable n-type carbon nanotube field-effect transistors. J Am Chem Soc 2001;123:11512–3.
[20] Kim HS, Yoon SH, Kwon SM, Jin HJ. pH-sensitive multiwalled carbon nanotube dispersion with silk fibroins. Biomacromolecules 2009;10(1):82–6.
[21] Zheng M, Jagota A, Semke ED, Diner BA, Mclean RS, Lustig SR, et al. DNA-assisted dispersion and separation of carbon nanotubes. Nat Mater 2003;2:338–42.
[22] Matsuura K, Saito T, Okazaki T, Ohshima S, Yumura M, Iijima S. Size-dependent melting properties of tin nanoparticles. Chem Phys Lett 2006;429:492–7.
[23] Tsyboulski DA, Bakota EL, Witus LS, Rocha JD, Hartgerink JD, Weisman RB. Self-assembling peptide coatings designed for highly luminescent suspension of single-walled carbon nanotubes. J Am Chem Soc 2008;130:17134–5.
[24] Zheng M, Jagota A, Strano MS, Santos AP, Barone P, Chou SG, et al. Structure-based carbon nanotube sorting by sequence-dependent DNA assembly. Science 2003;302:1545–8.

[25] Wu P, Chen X, Hu N, Tam UC, Blixt O, Zettl A, et al. Biocompatible carbon nanotubes generated by functionalization with glycodendrimers. Angew Chem Int Ed 2008;47:5022–5.
[26] Zeng HL, Gao C, Yan D. Poly(ϵ-caprolactone)-functionalized carbon nanotubes and their biodegradation properties. Adv Funct Mater 2006;16:812–8.
[27] Huang W, Taylor S, Fu K, Lin Y, Zhang D, Hanks TW, et al. Attaching proteins to carbon nanotubes via diimide-activated amidation. Nano Lett 2002;2:311–4.
[28] Fu K, Huang W, Lin Y, Zhang D, Hanks TW, Rao AM, et al. Functionalization of carbon nanotubes with bovine serum albumin in homogeneous aqueous soultions. J Nanosci Nanotechnol 2002;2:457–61.
[29] Liu Z, Winters M, Holodniy M, Dai H. siRNA Delivery into human T cells and primary cells with carbon-nanotube transporters. Angew Chem Int Ed 2007;46:2023–7.
[30] Yang ST, Fernando KA, Liu JH, Wang J, Sun HF, Liu YF, et al. Covalently PEGylated carbon nanotubes with stealth character *in vivo*. Small 2008;4:940–4.
[31] Hench LL. Bioceramics. J Am Ceram Soc 1998;81:1705–28.
[32] Kantesh B, Rebecca A, Tapas L, Melanie A, Jorge T, Eric C, et al. Plasma-sprayed carbon nanotube reinforced hydroxyapatite coatings and their interaction with human osteoblasts *in vitro*. Biomaterials 2007;28:618–24.
[33] Kantesh B, Yao C, Sandip PH, Narendra BD, Arvind A. Tribological behavior of plasma-sprayed carbon nanotube-reinforced hydroxyapatite coating in physiological solution. Acta Biomater 2007;3:944–51.
[34] Liao Susan, Guofu X, Wei W, Fumio W, Fuzhai C, Seeram R, et al. Self-assembly of nano-hydroxyapatite on multi-walled carbon nanotubes. Acta Biomater 2007;3:669–75.
[35] Hofle VG, Steiglich W, Vorbrüggen H. 4-Dialkylaminopyridine als hochwirksame acylierungskatalysatoren. Angew Chemie 1978;90:602–15.
[36] Danahy MP, Avaltroni JK, Midwood S, Schwarzbauer JE, Schwartz J. Self-assembled monolayers of a, w-diphosphonic acids on Ti enable complete or spatially controlled surface derivatization. Langmuir 2004;20:5333–7.
[37] Deckers AS, Gouget B, L'Hermite MM, Boime NH. In vitro investigation of oxide nanoparticle and carbon nanotube toxicity and intracellular accumulation in A549 human pneumocytes. Toxicology 2008;253:137–46.
[38] Datsyuk V, Kalyva M, Papagelis K, Parthenios J, Tasis D, Siokou A, et al. Chemical oxidation of multiwalled carbon nanotubes. Carbon 2008;46:833–40.
[39] Xu AW, Ma Y, Cölfen H. Biomimetic mineralization. J Mater Chem 2007;17:415–49.
[40] Tsukasa A, Fumio W, Yoshinori S, Kazuyuki T. Apatite formation on carbon nanotubes. Mater Sci Eng C 2006;26:675–8.
[41] James DK, Antonios G. Review: mineralization of synthetic polymer scaffold for bone tissue engineering. Tissue Eng 2007;13:927–38.
[42] Tanahashi M, Matsuda T. Surface functional group dependence on apatite formation on self-assembled monolayers in a simulated body fluid. J Biomed Mater Res 1997;34:305–15.
[43] Boskey AL, Posner AS. The role of synthetic and bone extracted Ca–phospholipid-PO_4 complexes in hydroxyapatite formation. Calcif Tissue Res 1997;23:251–8.
[44] Chang MC, Douglas WH, Tanaka J. Organic-inorganic interaction and the growth mechanism of hydroxyapatite crystals in gelatin matrices between 37 and 80 °C. J Mater Sci Mater Med 2006;17:387–96.
[45] Kato K, Eika Y, Ikada Y. In situ hydroxyapatite crystallization for the formation of hydroxyapatite/polymer composites. J Mater Sci 1997;32:5533–43.
[46] Zheng XT, Zhou SB, Xiao Y, Yu XJ, Feng B. In situ preparation and characterization of a novel gelatin/poly(D, L-lactide)/hydroxyapatite nanocomposite. J Biom Mater Res B 2009;91B:181–90.
[47] Liu TY, Chen SY, Liu DM, Liou SC. On the stury of BSA-loaded calcium-deficient hydroxyapatite nano-carriers for controlled drug delivery. J Control Release 2005;107:112–21.
[48] Joschek S, Nies B, Krotz R, Gopferich A. Chemical and physicochemical characterization of porous hydroxyapatite ceramics made of natural bone. Biomaterials 2000;21:1645–58.
[49] Hossaing SF, Hubbell JA. Molecular weight dependence of calcification of polyethylene glycol hydrogels. Biomaterials 1994;15:921–5.
[50] Qiu CF, Xiao XF, Liu RF. Biomimetic synthesis of spherical nano-hydroxyapatite in the presence of polyethylene glycol. Ceram Int 2008;34:1747–51.